Performance Improvement of Energy Efficient Five-Phase Permanent-Magnet Motor Drives

*1.A.MOHAMED ASIF M.E.,(ENERGY ENGG),AVCCE

*2.R.SELVA GANAPATHY,ASST,PROFESSOR(EEE),AVCCE

*3.A.PRIYANKA M.E.,(ENERGY ENGG),AVCCE

*4.G.ASHOK KUMAR, ASST,PROFESSOR(EEE),AVCCE

ABSTRACT

In this paper, a five-phase brushless permanent-magnet (PM) motor is introduced. The proposed motor has concentrated windings such that the produced back electro-motive force is almost trapezoidal. The motor is supplied with the combined sinusoidal plus third harmonic of currents. This motor, while generating the same average torque as an equivalent PM brushless dc motor (BLDC), overcomes its disadvantages. The motor equations are obtained in the d111 d3130 rotating reference frame. Therefore, the so-called vector control is easily applicable to this kind of motors and the motor has the same controllability as a PM synchronous motor (PMSM). For presenting the superior performance of the proposed five-phase motor, its three and five-phase PMSM and BLDC counterparts are also analyzed. Finite element method is used for studying the flux density and calculating the developed static torque. Also, the developed torque is obtained using the mathematical model in the d-1 reference frame. The average torque and the torque ripple for all cases are calculated and compared. Experimental results are in good agreement with the simulation results.

Keywords—Finite-element analysis, five-phase permanent-magnet (PM) motor, rotating reference frame, vector control.

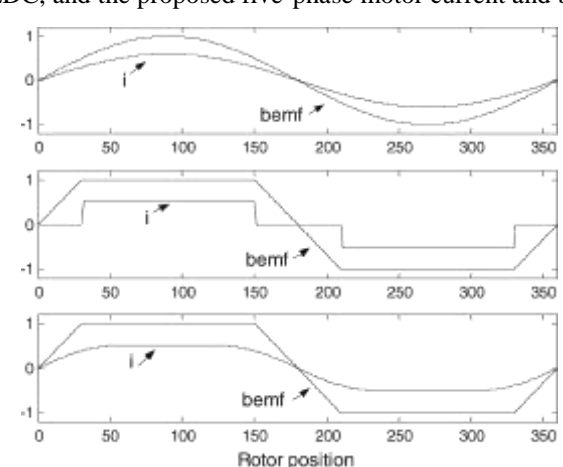


Fig. 1. Top to bottom: PMSM, BLDC, and the proposed five-phase motor current and back-EMF waveforms.

I.INTRODUCTION

The permanent-magnet ac (PMAC) motors are classified into sinusoidally fed PM synchronous motors (PMSMs)and rectangular-fed brushless dc (BLDC) PM motors [1], [2]. The stator winding of a PMSM motor is wound such that the back electromotive force (EMF) is sinusoidal. Therefore, a sinusoidal phase current produces constant torque. The stator winding in a BLDC motor is wound such that the back EMF is trapezoidal. In order to produce constant torque, quasi-rectan-gular currents should be supplied to the motor. BLDC motors benefit from higher torque density in comparison with PMSMs below rated speed. However, the BLDC operation above rated speed is being performed by advance angle technique. In this method, turning on each phase sooner allows the current to build up before the back EMF reaches its maximum value. This method has proved useful in some cases. However, it is difficult to achieve quantitative speed or torque control as compared with a PMSM drive in the flux-weakening region. In other words, either at a given torque or a given speed, it Paper IPCSD-04-068, presented at the 2003 Industry Applications Society Annual Meeting, Salt Lake City, UT, October 12–16, and approved for publication in the IEEE TRANSACTIONS ON INDUSTRY APPLICATIONS by the Electric Machines Committee of the IEEE Industry Applications Society. Manuscript submitted for review December 19, 2003 and released for publication October 8, 2004.

The authors are with the Advanced Electric Machines and Power Electronics Laboratory, Department of Electrical Engineering, Texas A&M University, College Station, TX 77843-3128 USA (e-mail: leila@ee.tamu.edu; toliyat@ee.tamu.edu).

Digital Object Identifier 10.1109/TIA.2004.841021 is difficult to find the exact advance angle to be applied. On the other hand, the stator winding inductances can cause the phase current to deviate significantly from the ideal rectangular waveform which will reduce the torque production capability at high speeds.

In sinusoidally fed PMSMs the torque-producing and flux-producing component of the current have been decoupled based on the *d*-*1* transformation. More advanced control techniques such as vector control are applicable to these drives, therefore, they have better controllability over the complete speed range.

Previously, third harmonic of current has been used to in-crease the specific torque of induction and synchronous reluctance machines. These machines were capable of developing more torque for the same amount of copper and iron as equivalent three-phase induction, and synchronous reluctance motors [3], [4].

Considering the above-mentioned points, a new five-phase brushless PM (5BPM) motor is proposed. The stator is wound such that the induced back EMF is quasi-rectangular and is sup-plied by combined sinusoidal and third harmonic current which nearly replicates a rectangular waveform as shown in Fig. 1. The mathematical model of the motor is derived in the difficial 0 rotating reference frame. Vector control is easily applicable to this kind of drive. The motor uses the advantages of both BLDC motor and PMSM. This means that it uses the controllability of a PMSM while having the high torque density of a BLDC motor.

Besides providing the ability of injecting third harmonic component of current and increasing the torque production capability of the motor, multiphase motor drives posses many other advantages over the traditional three-phase motor drives such as reducing the amplitude and increasing the frequency of torque

International Journal of Advance Research in Science and Engineering

Volume No.07, Special Issue No.06, March 2018

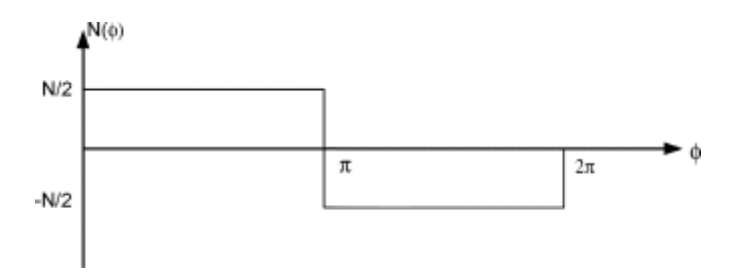
www.ijarse.com

PARSA AND TOLIYAT: FIVE-PHASE PM MOTOR DRIVES

31

ISSN: 2319-8354

Pulsations, reducing the stator current per phase without in-creasing the voltage per phase, and increasing the reliability [5]–[9]. The high phase order drive is likely to remain limited to specialized applications where high reliability is demanded such as electric/hybrid electric vehicles, aerospace applications, ship propulsion, and high-power applications where a combination of several solid-states device forms one leg of the drive. Therefore, the requirement of n separate drive units in a multiphase system is not oppressive for large drives since many of the necessary components are presented in the contemporary designs.



Nonlinear finite-element method [10] and dynamic simulation in MATLAB are presented to support the superior performance of the proposed motor compared to its BLDC and conventional PMSM counterparts. Five-phase PM motors and five-leg insulated-gate-bipolar-transistor (IGBT)-based inverters have been designed and fabricated in the laboratory. A Texas Instruments TMS320C32 floating-point digital signal processor (DSP) is used to implement the digital control. It is shown that the experimental results are in good agreement with simulation results.

II. MATHEMATICAL MODEL OF THE 5BPM MOTOR

In this section, the mathematical model of the five-phase motor will be derived and the voltage, flux, and torque equations will be established in the rotating reference frame.

The stator voltage equations are given by

$$d\Lambda$$

$$V_s = R_s I_s + \frac{s}{dt}$$
(1)

Where \mathbb{R} , \mathbb{I} , and $\Lambda_{\mathbb{R}}$ are the stator resistance, current, and flux linkages matrices, respectively.

The air-gap flux linkages are presented by

Volume No.07, Special Issue No.06, March 2018 Www.ijarse.com IJARSE ISSN: 2319-8354

$$\Lambda_s = \Lambda_{ss} + \Lambda_m$$
. (2)

Substituting for the flux linking stator windings due to the cur-rents in the stator windings in terms of the stator currents and stator winding inductances,

$$\Lambda_{\kappa} = L_{\kappa\kappa}I_{\kappa} + \Lambda_{m}. \qquad (3)$$

The stator currents are given by

$$I_s = [I_{as} \quad I_{bs} \quad I_{cs} \quad I_{ds} \quad I_{cs}]^t.$$
 (4)

 $L_{\pi\pi}$ is the stator inductance matrix which contains the self-

and mutual inductances of the stator phases, and \mathbb{R} is the established flux linkage matrix due to the PMs viewed from the stator phase windings. For simplifying the model, only the fundamental and third harmonic component of the magnet flux linkage is taken into account. Considering this approximation \mathbb{R} can be written as follows:

$$\begin{bmatrix} \sin(\theta_r) \\ \sin\left(\theta_r - \frac{2\pi}{5}\right) \\ \left(& 4 \end{bmatrix} \end{bmatrix} \begin{bmatrix} \sin(3\theta_r) \\ \sin 3\left(\theta_r - \frac{2\pi}{5}\right) \\ \left(& 4 \end{bmatrix} \end{bmatrix}$$

$$\Lambda_m = \lambda_{m1} \begin{bmatrix} \sin \theta_r - \frac{\pi}{5} \\ \sin \left(\theta_r + \frac{4\pi}{5}\right) \\ \sin \left(\theta_r + \frac{2\pi}{5}\right) \end{bmatrix} + \lambda_{m3} \begin{bmatrix} \sin 3 \theta_r - \frac{\pi}{5} \\ \sin 3 \left(\theta_r + \frac{4\pi}{5}\right) \\ \sin 3 \left(\theta_r + \frac{2\pi}{5}\right) \end{bmatrix}.$$
 (5)

Fig. 2. Stator phase winding function.

 λ_{m1} and λ_{m3} are the amplitude of fundamental and third harmonic components of magnet flux linkages and θ_r is the rotor position.

As previously mentioned, this motor has concentrated windings as depicted in Fig. 2 where the air gap is assumed to be uniform. The self- and mutual inductances of the stator have constant values. In order to simplify the modelling, only the fundamental and the third harmonic components of the winding functions are considered. The Fourier series of the winding function for phase "a" can be written as follows:

$$4 N \begin{bmatrix} 1 \\ N_a(\varphi) = \frac{s}{\pi} \frac{s}{P} \cos(\phi) - \frac{1}{3}\cos(3\phi) \end{cases}$$
(6)

Where $\mathbb N$ the total number of turns is, P is the number of poles, and $\mathbb P$ is the spatial angle. The winding functions of other phases are shifted by 72 electrical degrees with respect to each other.

The self- and mutual inductances of the stator phases can be computed by using the corresponding winding functions and are given by

$$L_{aa} = L_{bb} = L_{cc} = L_{dd} = L_{ce}$$

$$= \frac{\mu \circ rl}{g} \pi N_{s1}^2 + \frac{\mu \circ rl}{g} \pi N_{s3}^2$$

$$= L_{ms1} + L_{ms3}$$

$$L_{abs} = L_{bcs} = L_{cds} = L_{des}$$

$$= L_{acs} = \cos \frac{2\pi}{5} L_{ms1} + \cos 3 \frac{2\pi}{5} L_{ms3}$$

$$L_{acs} = L_{bds} = L_{ces} = L_{das}$$

$$4\pi$$

$$= L_{cbs} = \cos \frac{1}{5} L_{ms1} + \cos 3 \frac{1}{5} L_{ms3}$$
 (7)

where

$$N_{s1} = \frac{4}{\pi} \frac{N_s}{P}$$

$$1 \ 4 \ N$$

$$N_{s3} = -\frac{1}{3\pi} \frac{s}{P}.$$
 (8)

To simplify the machine model, an arbitrary coordinate transformation is introduced, which transfers the variables of the five-phase motor into a reference frame rotating at an arbitrary angular velocity. Including the effect of third harmonic,

a di-Ti-di-Ti-n transformation can be applied. The di-Ti coordinate is rotating at synchronous speed and the di-Ti coordinate is rotating at three times the synchronous speed. The transformation matrix for this system is considered as (9), shown at the bottom of the next page.

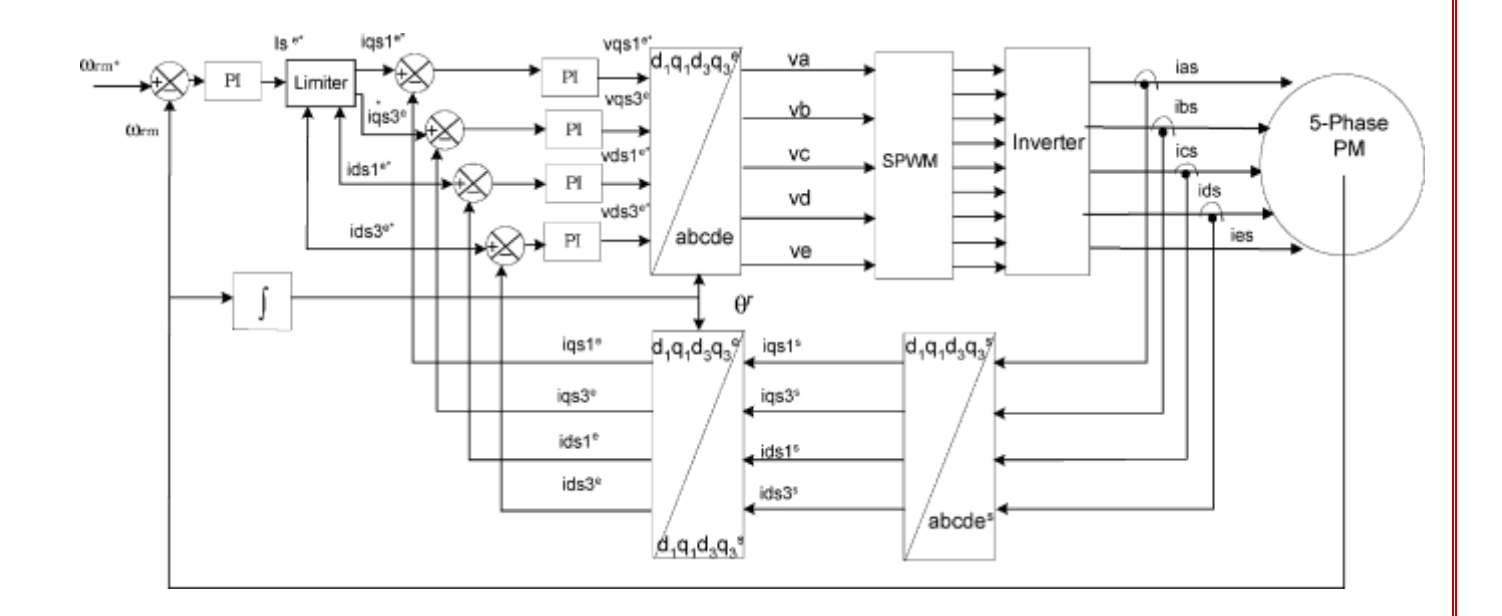


Fig. 3. Complete control block diagram.

By applying this transformation to the stator voltages and flux linkages equations and calculating the torque, the following equations will be obtained:

Stator voltages:

 $d\lambda_{d-1}$



where W_0 is the co-energy and θ_{rm} is the mechanical rotor angle. The co-energy is defined as follows: 1 (19) $W_{co} = \frac{1}{2}I_s^T L_s I_s + I_s^T \Lambda_m.$ Taking the partial derivative of the co-energy with respect to yields (11)(20)(12)or (13)(21) where stator flux linkages are given by The transformation matrix has the following pseudo-orthogonal (14)property: (15)(22) (16)therefore, (17)(23)The electromagnetic torque is determined by and, finally, (18)(24)

International Journal of Advance Research in Science and Engineering

Volume No.07, Special Issue No.06, March 2018

www.ijarse.com

HARSE ISSN: 2319-8354

 $V_{ds1} = r_s i_{ds1} - \omega \lambda_{qs1} + \frac{s}{dt}$ $V_{qs1} = r_s i_{qs1} + \omega \lambda_{ds1} + \frac{d\lambda_{qs1}}{dt}$ $V_{ds3} = r_s i_{ds3} - 3\omega \lambda_{qs3} + \frac{d\lambda_{ds3}}{dt}$

$$T_{c} = \frac{P}{2} I_{s}^{T} \frac{\partial \Lambda_{m}}{\partial \theta_{r}}$$

$$V_{ds3} = r_s i_{ds3} - 3\omega \lambda_{qs3} + dt$$

 $V_{qs3} = r_s i_{qs3} + 3\omega \lambda_{ds3} + d\lambda_{qs3}$

$$T_e = \frac{P}{2} (T(\theta_r)^{-1} i_{d1q1d3q30s})^t \frac{\partial \Lambda_m}{\partial \theta_r}.$$

$$\begin{split} \lambda_{ds1} &= \left(L_{\ell s} + \frac{5}{2} L_{ms1}\right) i_{ds1} + \lambda_{m1} \\ \lambda_{qs1} &= \left(L_{\ell s} + \frac{5}{2} L_{ms1}\right) i_{qs1} \\ \lambda_{ds3} &= \left(L_{\ell s} + \frac{5}{2} L_{ms3}\right) i_{ds3} + \lambda_{m3} \\ \lambda_{qs3} &= \left(L_{\ell s} + \frac{5}{2} L_{ms3}\right) i_{qs3}. \end{split}$$

$$T^{-1}(\theta_r) = \frac{5}{2} T^t(\theta_r)$$

$$T_c = \frac{\partial W_{co}}{\partial \theta_{rm}}$$

$$T_e = \frac{5}{2} \frac{P}{2} i_{d1q1d3q30s} {}^t T(\theta_r) \frac{\partial \Lambda_m}{\partial \theta_r}$$

$$T_{c} = \frac{5}{2} \frac{P}{2} [\lambda_{m1} i_{qs1} + 3\lambda_{m3} i_{qs3}].$$

$$2\begin{bmatrix} \sin\theta_r & \sin(\theta_r - \frac{2\pi}{5}) & \sin(\theta_r - \frac{4\pi}{5}) & \sin(\theta_r + \frac{4\pi}{5}) & \sin(\theta_r + \frac{2\pi}{5}) \\ \cos\theta_r & \cos(\theta_r - \frac{2\pi}{5}) & \cos(\theta_r - \frac{4\pi}{5}) & \cos(\theta_r + \frac{4\pi}{5}) & \cos(\theta_r + \frac{2\pi}{5}) \\ & & & & & & & & & & & & & & & \\ \end{bmatrix}$$

$$T(\theta_r) = \frac{1}{5} \begin{bmatrix} \sin 3\theta_r & \sin 3 \ \theta_r - \frac{\pi}{5} & \sin 3 \ \theta_r - \frac{\pi}{5} & \sin 3 \ \theta_r + \frac{\pi}{5} \\ \cos 3\theta_r & \cos 3 \left(\theta_r - \frac{2\pi}{5}\right) & \cos 3 \left(\theta_r - \frac{4\pi}{5}\right) & \cos 3 \left(\theta_r + \frac{4\pi}{5}\right) \\ \frac{1}{\sqrt{2}} & \frac{1}{\sqrt{2}} & \frac{1}{\sqrt{2}} \end{bmatrix}$$

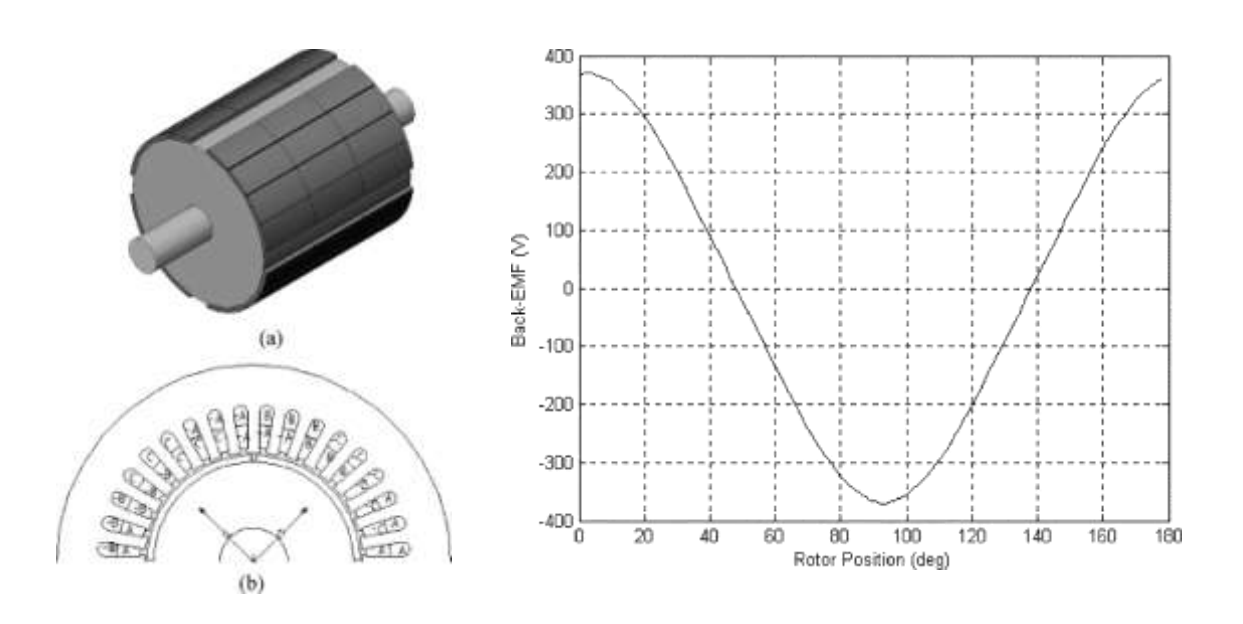
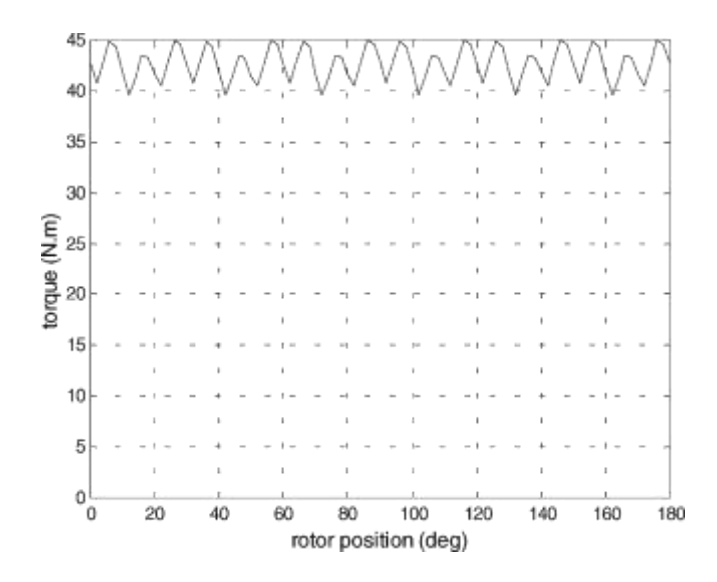


Fig. 5. Back EMF of 36-slot three-phase PMSM motor.

Fig. 4. Three-phase PMSM motor. (a) PM rotor. (b) PM motor cross section.



ISSN: 2319-8354

Substituting from (14)–(17)

$$\begin{split} T_c &= \frac{5}{2} \frac{P}{2} \bigg\{ \left[\left[\lambda_{ds1} - \left(L_{ls} + \frac{5}{2} L_{ms1} \right) i_{ds1} \right] i_{qs1} \right] \\ &+ \left[3 \left[\lambda_{ds3} - \left(L_{ls} + \frac{5}{2} L_{ms3} \right) i_{ds3} \right] i_{qs3} \right] \bigg\}. \end{split}$$

The electromagnetic torque can be written as

$$T_c = \frac{1}{4} (\lambda_{ds1} i_{qs1} - \lambda_{qs1} i_{ds1} + 3\lambda_{ds3} i_{qs3} - 3\lambda_{qs3} i_{ds3})$$
(25)

where λ_{dal} , λ_{al} , λ_{dal} , and λ_{al} are the stator fluxes in the dl,

II, do, and I axes, respectively. ideal, iel, ideal, and ield are the transformed stator currents in these rotating axes. The improvement in the developed torque due to the third harmonic can be noticed from (25). As can be understood from the equations, the so-called vector control is easily applicable to this kind of motor. Fig. 3 shows the control block diagram of the proposed motor where the difference between the reference speed and the actual speed determines the reference stator currents in the rotor reference frame. The reference stator voltages in the rotating reference frame are generated by the associated proportional plus integral (PI) current regulator based on the difference between the commanded currents and the transformed sensed currents. Sinusoidal pulse width-modulation (PWM) technique has been used to drive the inverter.

III.FINITE-ELEMENT AND DYNAMIC ANALYSIS

Simulations have been performed using both finite element method and MATLAB/Simulink to verify the superior performance of the proposed motor. A three-phase 7.5-hp four-pole 460-V 10-A 36-slot off-the-shelf induction motor is used for this study. The rotor of this motor has been replaced with a PM rotor as shown in Fig. 4(a). In each pole, 12 pieces of magnets are used. Fig. 4(b) illustrates the cross section of the PMSM motor which was built on the same stator frame as the induction motor, and is used as our reference motor. The magnets are NdFeBr of type

ISSN: 2319-8354

Volume No.07, Special Issue No.06, March 2018 Www.ijarse.com IJARSE ISSN: 2319-8354

Fig. 6. Torque of the 36-slot PMSM motor.

35EH with B = 1.21 T. The stator coil pitch is 7/9, and the number of turns per coil is 30. The stator outer diameter, inner diameter, rotor outer diameter, shaft outer diameter, and stack length are 228.6, 127, 124, 40, and 101.6 mm, respectively.

The induced back EMF of coil A which is calculated from the flux linking coil A using the Ansoft finiteelement package is shown in Fig. 5. The system uses virtual work principles to compute the torque on an object

$$\partial W \qquad \partial \left[\int \left(\int^{H} \right) \cdot V \right]$$

$$T = \frac{co}{\partial \theta_{rm}} = \frac{co}{\partial \theta_{rm}} = \frac{B \cdot dH}{V} \cdot d \qquad (26)$$

The motor has sinusoidal back EMF and is supplied with sinusoidal currents. The developed static torque is shown in Fig. 6. The average torque in this case is 42.62 N m. The torque pulsations due to the slots openings are clear. With a 12-slot stator, the back EMF is quasi-rectangular and the motor can be supplied with current pulses of 120₀ to produce almost constant torque. The developed torque using finite element is 46.9 N m. The torque is 10% higher than the 36-slot PMSM.34

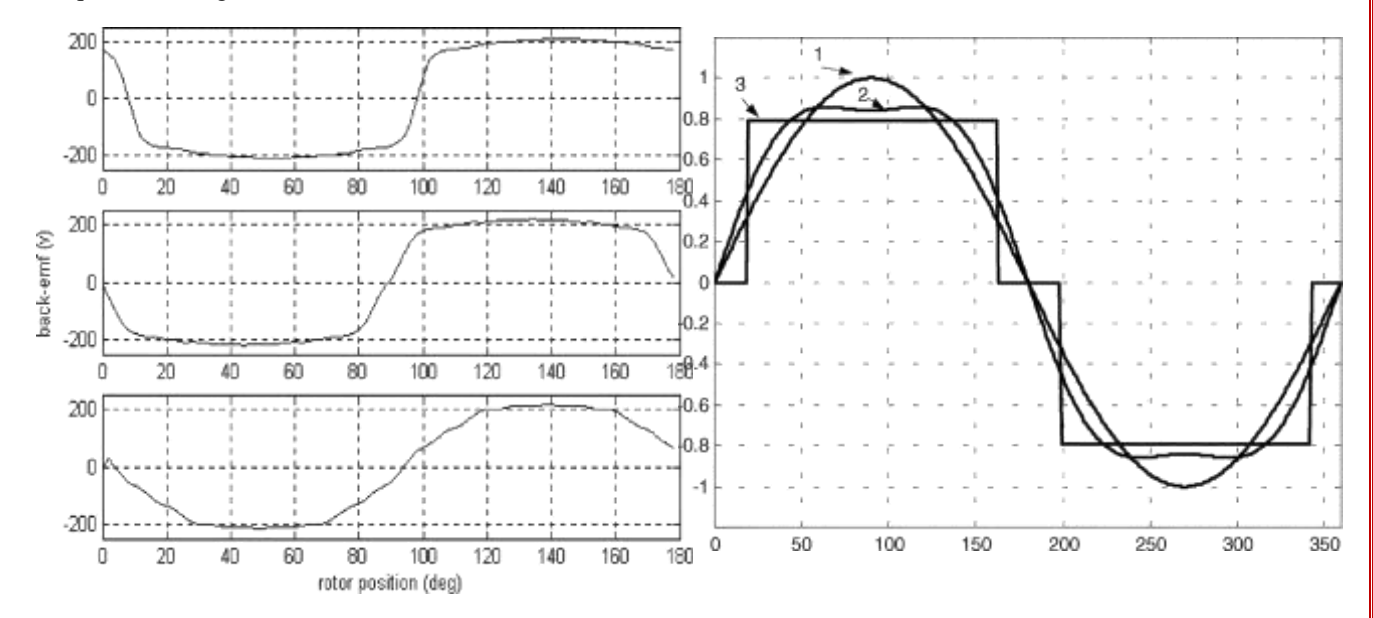


Fig. 8. Top to bottom: back EMF of 20-slot, 40-slot single-layer, and 40-slot double-layer five-phase machines

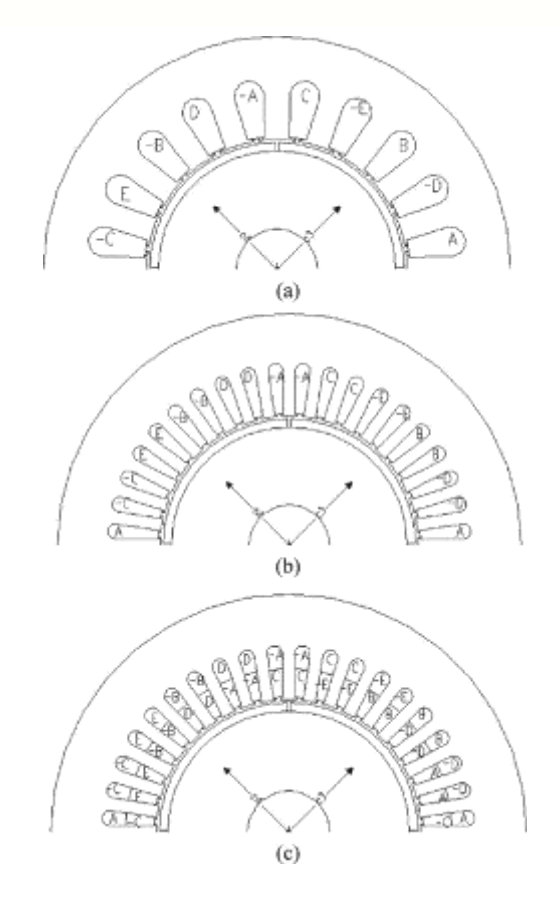


Fig. 7. Cross section of five -phase, (a) 20-slot, (b) 40-slot single layer, and (c) 40-slot double layer.

The five-phase 20-slot, the 40-slot single-layer which is used for experimental verifications, and the 40-slot double-layer motors have been designed using the same frame size as the original three-phase motor. The number of turns and slot widths has been adjusted to maintain almost the same amount of copper and iron and, therefore, almost equal copper and core losses are maintained. The performance of five-phase 20-slot, 40-slot single-layer, and 40-slot double-layer PM motors is compared. In this study, the motors with quasi-rectangular back EMF are supplied with both combined fundamental and third harmonic of current and current pulses of 144a with four phases conducting at each instant of time. In this way, it can be shown that both kinds of excitation will generate almost the same output torque while those supplied with combined fundamental and third harmonic of current have better controllability due to vector control.

The 40-slot double-layer motor has been considered as the reference for comparing the five-phase conventional sinusoidally fed PMSM with the motors supplied with fundamental and third harmonic of currents. Fig. 7 shows the cross section and winding distribution of all three motors. Fig. 8 shows the back-EMF waveforms of these motors. The back EMF of the 20-slot motor is trapezoidal. It progresses toward sinusoidal

waveform as the number of stator slots increases to 40 slots, and the number of layers changes from single to double layer.

The developed torques of all the motors supplied with different current waveforms has been obtained using the finite-element method. In each case, the peak values of

Fig. 9. (1) Sinusoidal, (2) combined sinusoidal and third harmonic, and (3) 144₄ pulses of current with the same rms values.

Current have been adjusted so that the rms current for all the cases is kept the same as shown in Fig. 9. The amount of the injected third harmonic of current is 15% of the fundamental frequency current. From Fig. 9, it is clear that the 144^a pulse of current has the lowest peak value among all the three types of currents. The 20-slot and the 40-slot single-layer motors with quasi-rectangular back EMF have been supplied with both 144^a current pulses, and the combined fundamental and third harmonic of currents. The double-layer 40-slot motor has been supplied with sinusoidal current. The static torques of these motors with different excitation currents under rated condition are shown in Fig. 10. From Figs. 6 and 10, the developed torques by five-phase 20-slot and 40-slot single-layer motors are higher than that of the three-phase 36-slot and five-phase double-layer 40-slot PMSMs. Fig. 11 shows the torque-angle curve for the 40-slot single-layer motor when supplied with combined fundamental and third harmonic of rated and 50% of the rated

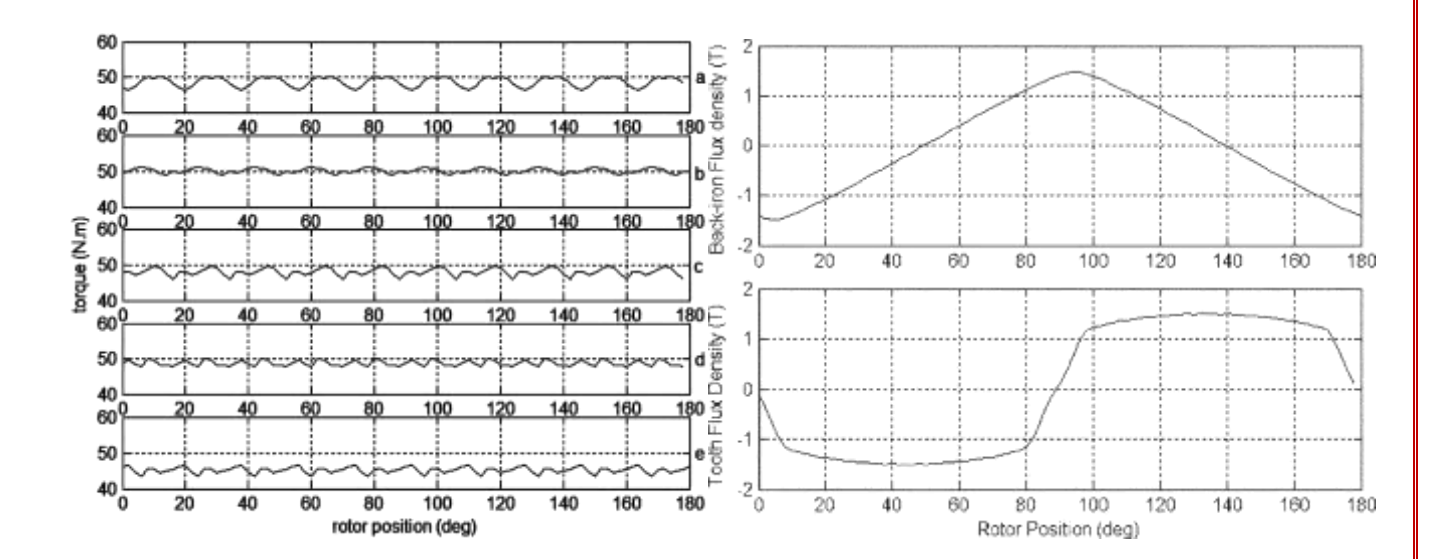


Fig. 10. Torque of (a) 20 stator slots motor supplied as BLDC, (b) 20-slot motor supplied with combined sinusoidal and third harmonic, (c) 40-slot single-layer motor supplied as BLDC, (d) 40-slot single-layer motor supplied with combined fundamental and third harmonic, and (e) 40-slot double-layer motor supplied with sine

currents.

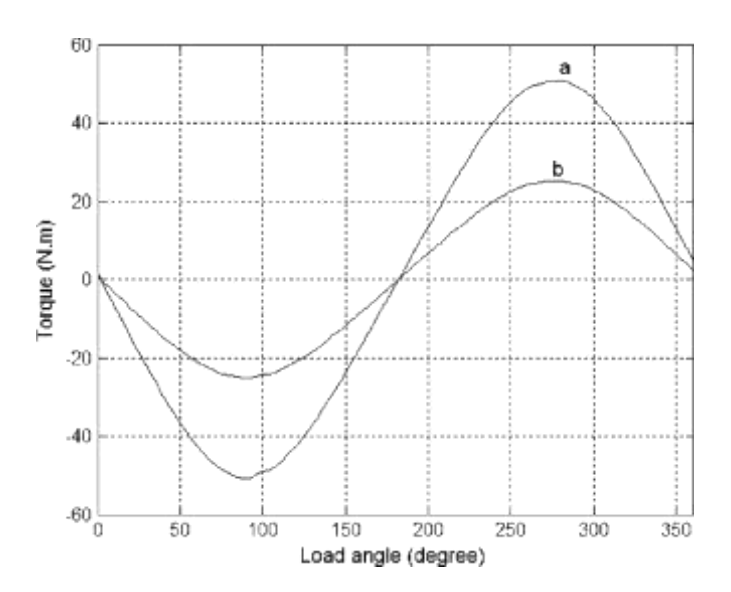


Fig. 11. Torque versus load angle curves for rated and 50% of the rated currents.

Current Fig. 12 presents the flux densities in the stator tooth and the stator back iron for the proposed five-phase 40-slot single-layer PM motor supplied with combined fundamental and third harmonic of currents. The tooth and back-iron flux densities of other motors have been calculated and presented in Table I together with the average torque and torque ripple of all the motors.

The developed torque can be computed using *d*—I transformation as explained in Section II. The results of digital computer simulations have been summarized in Table I as well. As can be seen from the table, the five-phase 20-slot motor supplied with the combined fundamental plus third harmonic of currents produces about 17.3% more torque with respect to the original three-phase PMSM. The proposed five-phase 40-slot motor supplied with the fundamental plus third harmonic of currents produces about 14.5% more torque than the original three-phase

Fig. 12. Top to bottom: tooth flux density, and back-iron flux density of 40-slot motor supplied with combined fundamental plus third harmonic of currents.

motor. The proposed five-phase motor (supplied with combined fundamental plus third harmonic of currents) has 10% more torque than the five- phase PMSM. The torque of the proposed motor is higher than its similar BLDC motor. However, since the peak current in the case of the BLDC motor is lower, the tooth flux density is lower as well. Also, it should be noted that the tooth and the back-iron flux densities in the proposed motor are lower than the PMSM counterpart.

In all cases, the flux densities in the tooth and back iron are within the acceptable range. The table also shows the torque ripple for all the motors. As expected, the torque ripples of the five-phase motors are lower than that of the three-phase and have higher frequencies. As mentioned earlier, the last column of the table shows the torque computed using the *d-1* model. From the table, it can be realized that the torque values agree well with those calculated using the finite-element package. It should be mentioned that the percentages of torque improvement of five-phase 20-slot and 40-slot motors with respect to that of the three-phase 36-slot motor are in fact a few percent lower than those numbers calculated above since the effect of end-windings lengths has been neglected. Considering the effect of end windings on the number of turns, the torque improvement of the proposed five-phase 40-slot motor with respect to the three-phase motor decreases from 14.5% to 12.4%. It is expected that the torque improvement of the five-phase 20-slot motor compared to the 36-slot motor which initially was calculated to be 17.3% should also drop by a few percent after considering the end-windings effect.

IV. EXPERIMENTAL RESULTS

The five-phase PM motor has been fabricated in the laboratory. Fig. 13 shows the rotor made from small pieces of loaf magnets and the five-phase stator. The five-leg IGBT-based inverter has also been fabricated in the laboratory. The TMS320C32 floating-point DSP is used to implement the digital control.

This motor is supplied with combined sinusoidal and third harmonic of current. Fig. 14 shows the current waveform and the

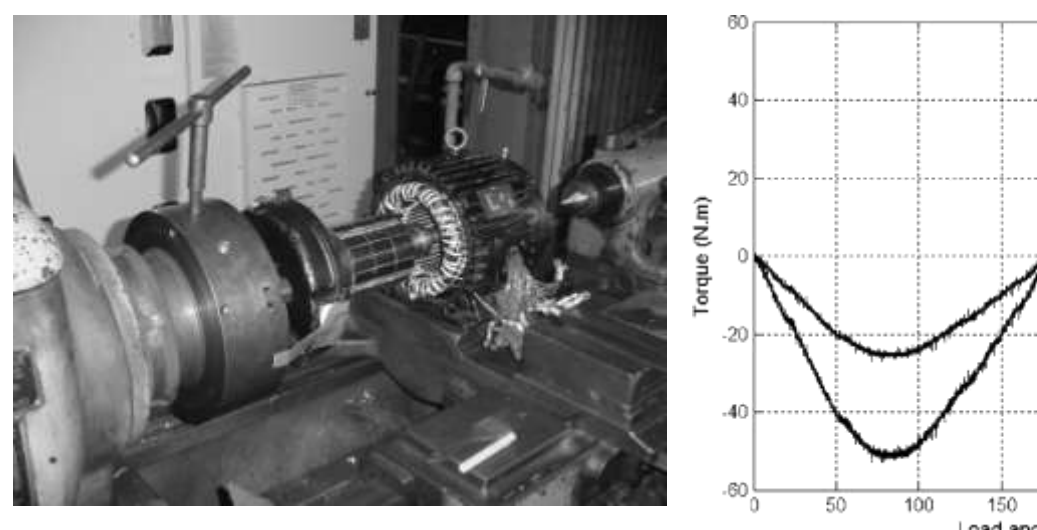
TABLE I SUMMARY OF SIMULATION RESULTS

Motor type	Current type	Ave Torque	Torque	Tooth flux	Back-iron flux	Ave. torque
		from FE	ripple%	density	density	from d-q model
3 phase 36 slots	Sine	42.62	6.37%	1.54	1.57	43.31
3. phase 12 slots	120 (deg) pulses	46.9	8.5%	1.53	1.567	47.1
5 phase 20 slots	144 (deg) pulses	49.6	4%	1.551	1.492	50.12
5 phase 20 slots	Sine+3rd h	50	3.86%	1.558	1.498	50.9
5 phase 40 slots single layer	144 (deg) pulses	48	4.3%	1.545	1.484	48.7
5 phase 40 slots single layer	Sine+3rd h	48.8	3.72%	1.55	1.49	49.5
5 phase 40 slot double layers	Sine	44.2	3.4%	1.56	1.5070	44.6

International Journal of Advance Research in Science and Engineering 4 Volume No.07, Special Issue No.06, March 2018

www.ijarse.com





300 350 Load angle (degree)

Fig. 13.Rotor and stator of the 5BPM motor during assembly.

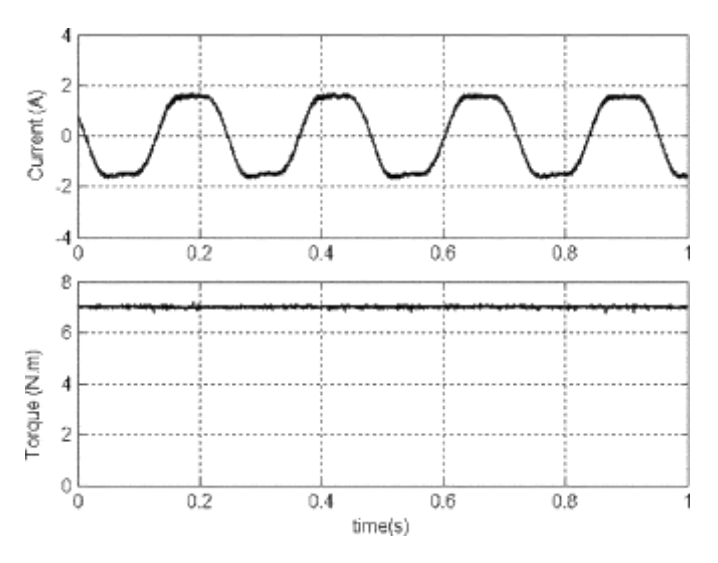


Fig. 15.Torque versus load angle curve.

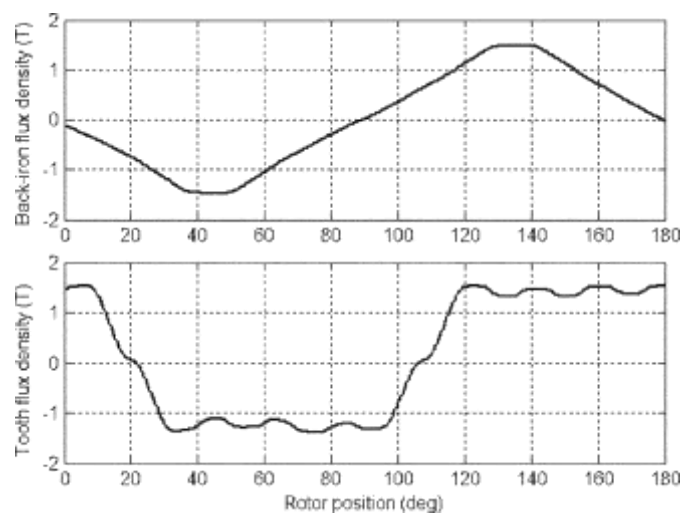


Fig. 14.Top to bottom: Stator phase current and output torque.

Fig. 16.Top to bottom: Back-iron and tooth flux densities.

produced output torque of the motor. The rms value of the cur-rent in this case is 1.4 A, and the produced torque is 7 N m. The torque obtained from the finite-element package under the same condition is 6.84 N m. Fig. 15 shows the torque-angle curve of the motor under rated and 50% of the rated current. This figure is in good agreement with Fig. 11 which has been obtained from the finite-element study. For the rated current, the peak torque from finite element is 50.6 N m and from experiment is 51.1 N m. For 50% of the rated current, the peak torque from finite element is 25.1 N m and from experiment is 25.4 N m. The tooth

flux density and the back-iron flux densities have also been monitored and are shown in Fig. 16. It is clear from these figures that these two waveforms are in good agreement with those obtained from the finite element shown in Fig. 12(a) and (b).

CONCLUSION

This paper has analyzed a new 5BPM motor, which has near-trapezoidal back EMF and is supplied with the combined fundamental plus third harmonic of currents. The flux and torque

\ equations have been obtained in an arbitrary rotating *d-II* reference frame. The performance of the proposed motor has been evaluated with respect to its three-phase and five-phase PMSM and BLDC counterparts. Finite-element method has been used for calculating the back EMF, the static torque, and the flux densities in the stator tooth and back iron

The results of dynamic simulation using the *d*-**T** model have been verified with finite-element results. The superior performance of the new five-phase motor compared to the PMSM ma-chine has been shown. This motor has better performance than the BLDC motor due to its controllability and compatibility with vector control technique, especially for high-speed applications and also during the field-weakening region. Experimental results were provided to support the theoretical findings.

ACKNOWLEDGMENT

The authors would like to sincerely thank Dr. A. Goodarzi of US Hybrid for the assistance provided with the experimental setup and Ansoft Company for the finite-element package.

REFERENCES

[1] P. Pillay and R. Krishnan, "Modelling, simulation, and analysis of per-manent-magnet motor drives, II-The brushless DC motor drive," *IEEE Trans. Ind. Appl.*, vol. 25, no. 2, pp. 274–279, Mar./Apr. 1989.

- [2] T. M. Jahns, "Motion control with permanent-magnet AC machines," *Proc. IEEE*, vol. 82, no. 8, pp. 1241–1252, Aug. 1994.
- [3] H. Xu, H. A. Toliyat, and L. J. Peterson, "Five-phase induction motor drives with DSP-based control systems," *IEEE Trans. Power Electron.*, vol. 17, no. 4, pp. 524–533, Jul. 2002.
- [4] R. Shi, H. A. Toliyat, and A. El-Antably, "Field oriented control of five-phase synchronous reluctance motor drive with flexible 3rd harmonic current injection for high specific torque," in *Conf. Rec. IEEE-IAS Annu. Meeting*, vol. 3, Chicago, IL, Sep. 30 Oct. 5, 2001, pp. 2097–2103.
- [5] T. Gopalarathnam, S. Waikar, H. A. Toliyat, M. S. Arefeen, and J. C. Moreira, "Development of low cost multi-phase brushless permanent magnet (BPM) motors with unipolar current excitations," in *Conf. Rec. IEEE-IAS Annu. Meeting*, Phoenix, AZ, Oct. 3–7, 1999, pp. 173–179.
- [6] P. J. McCleer, J. M. Bailey, J. S. Lawler, and B. Banerjee, "Five phase trapeziodal back EMF PM synchronous machines and drives," in *Proc. Eur. Conf. Power Electronics and Applications*, Sep. 1991, pp. 128–133.
- [7] C. C. Chan *et al.*, "A novel high power density permanent magnet variable-speed motor," *IEEE Trans. Energy Convers.*, vol. 8, no. 2, pp. 297–303, Jun. 1993.
- [8] F. Caricchi *et al.*, "Innovative inverter topology for concentrated winding PM motor drives," *Proc. IEEE PESC'92*, vol. 2, pp. 964–972, 1992.
- [9] H. A. Toliyat and L. Parsa, "Fault tolerant permanent magnet motor drives with high specific torque," U.S. Patent Disclosure 2093TEES04, Nov. 2003.
- [10] F. A. Fouad, T. W. Nehl, and N. A. Demerdash, "Magnetic field modelling of permanent magnet type electronically operated synchronous machine using finite elements," *IEEE Trans. Power App. Syst.*, vol. PAS-100, no. 9, pp. 4125–4135, Sep. 1981.